International Journal of Solids and Structures 47 (2010) 1118–1129

Contents lists available at ScienceDirect

International Journal of Solids and Structures

journal homepage: www.elsevier.com/locate/ijsolstr

Scattering of flexural wave in a thin plate with multiple circular holes by using the multipole Trefftz method

Wei-Ming Lee [a], Jeng-Tzong Chen [b,*]

[a] Department of Mechanical Engineering, China University of Science and Technology, Taipei, Taiwan
[b] Department of Harbor and River Engineering, National Taiwan Ocean University, Keelung, Taiwan

ARTICLE INFO

Article history:
Received 20 August 2009
Received in revised form 2 November 2009
Available online 21 December 2009

Keywords:
Scattering
Flexural wave
Plate
Dynamic moment concentration factor
Addition theorem

ABSTRACT

The scattering of flexural wave by multiple circular holes in an infinite thin plate is analytically solved by using the multipole Trefftz method. The dynamic moment concentration factor (DMCF) along the edge of circular holes is determined. Based on the addition theorem, the solution of the field represented by multiple coordinate systems centered at each circle can be transformed into one coordinate system centered at one circle, where the boundary conditions are given. In this way, a coupled infinite system of simultaneous linear algebraic equations is derived as an analytical model for the scattering of flexural wave by multiple holes in an infinite plate subject to the incident flexural wave. The formulation is general and is easily applicable to dealing with the problem containing multiple circular holes. Although the number of hole is not limited in our proposed method, the numerical results of an infinite plate with three circular holes are presented in the truncated finite system. The effects of both incident wave number and the central distance among circular holes on the DMCF are investigated. Numerical results show that the DMCF of three holes is larger than that of one, when the space among holes is small and meanwhile the specified direction of incident wave is subjected to the plate.

1. Introduction

Thin plates with multiple circular holes are widely used in engineering structures, e.g. missiles, aircraft, etc. Geometric discontinuities due to these holes result in the stress concentration, which significantly reduce the load carrying capacity. The deformation and corresponding stresses induced by dynamic loading are propagated throughout the structure by means of wave. At the irregular interface of different media, flexural wave scattered in all directions recursively interacts with the incident wave. It turns out that the scattering of the associated stress wave results in dynamic stress concentrations which are larger than static ones at certain wave frequencies (Pao and Mow, 1972).

Nishimura and Jimbo (1955) were two pioneers for the analytical study of the dynamic stress concentration and they determined the stresses in the vicinity of a spherical inclusion in the elastic solid under a harmonic force. Pao (1962) studied the scattering of flexural waves and dynamic stress concentrations around a circular hole, and proposed an analytical solution. Since then, most research work has focused on the scattering of elastic wave and the resulted dynamic stress concentration and has led to a rapid development of analytical or numerical approach such as the method of wave function expansion, the complex variable method, the boundary integral equation method and the boundary element method (Pao and Mow, 1972).

Kung (1964) studied dynamic stress concentrations resulting from the scattering of flexural waves on the thin plate with one circular hole and gave the calculations of moment and shear forces as a function of frequency. Liu et al. (1982) extended the complex variable function approach for statics to the case of dynamic loading. The dynamic stress concentration factors were given for circular and elliptical cavities in an infinite plane by incident plane compressional waves. By using the flux conservation relation and optical theorem, Norris and Vemula (1995) considered the scattering of flexural waves by circular inclusions with different plate properties and obtained numerical results. The complex variable function approach and conformal mapping technique were employed to solve the diffraction problem of flexural waves by two cutouts (Hu et al., 1998) and dynamic concentration factors of plates with two circular holes were presented under various boundary conditions. Squire and Dixon (2000) applied the wave function expansion method to study the scattering properties of a single coated cylindrical anomaly located in a thin plate on which flexural waves propagate. Gao et al. (2001) dealt with theoretical and numerical analysis of scattering of elastic wave and dynamic stress

* Corresponding author. Tel.: +886 2 24622192; fax: +886 2 24632375.
E-mail addresses: wmlee@cc.cust.edu.tw (W.-M. Lee), jtchen@mail.ntou.edu.tw (J.-T. Chen).

0020-7683/$ - see front matter © 2009 Elsevier Ltd. All rights reserved.
doi:10.1016/j.ijsolstr.2009.12.002

concentrations in an infinite plate with a circular hole using the boundary element method. Hayir and Bakirtas (2004) applied the image method to analyze the scattering and dynamic stress concentrations of elastic waves in plates with a circular hole subject to plane harmonic SH wave. Gao et al. (2005) studied the scattering of flexural waves and calculated the dynamic stress concentration in the thin plate with the cutout by using the dual reciprocity boundary element method. Hu et al. (2007) employed the wave function expansion and the expanded mode coefficients to represent the flexural wave scattered by a circular hole in a semi-infinite thin plate subject to the incident wave. According to the boundary conditions, these coefficients are recessively determined, which will become complicated and unmanageable as the number of holes increases. Consequently in their recent paper involving two circular holes (Fang et al., 2008), the total scattering coefficients (or simple coefficients) are used instead of the expanded mode coefficients. However, the proposed formulation is applicable to the case of two holes and is not general. Recently Lee and Chen (2008) proposed a semi-analytical approach to solve the flexural wave scattered by multiple holes in an infinite plate by using the null field integral equation method. In addition to the need of integration, this collocation method (Lee and Chen, 2008) belongs to point-matching approach instead of analytical derivation. It also increases the effort of computation since boundary nodes for collocation are required.

The Trefftz method was first presented by Trefftz (1926). On the boundary alone, this method was proposed to construct the solution space using trial complete functions which satisfy the given differential equation (Kamiya and Kita, 1995). Apparently, Trefftz method is categorized as the boundary-type solution such as the boundary element method (BEM) or boundary integral equation method (BIEM) which can reduce the dimension of the original problem by one and thus the number of the unknowns is much less than that of the domain type methods such as finite difference method (FDM) or finite element method (FEM). Moreover, the Trefftz formulation is regular and free of calculating improper boundary integrals. However, almost all the problems solved by using the Trefftz method are limited in the simply-connected domain. An extension to problems with multiple holes, i.e. multiply-connected domain, is our concern in this paper.

The concept of multipole method to solve multiply-connected domain problems was firstly devised by Zaviška (1913) and used for the interaction of waves with arrays of circular cylinders by Linton and Evans (1990). Recently, one monograph by Martin (2006) used these and other methods to solve problems of the multiple scattering in acoustics, electromagnetism, seismology and hydrodynamics. However, the BiHelmholtz problem with the fourth order differential equation was not mentioned therein.

This paper proposed the multipole Trefftz method to solve flexural waves scattered by multiple circular holes in an analytical way. When considering an infinite thin plate with multiple circular holes, the transverse displacement field is expressed as an infinite sum of multipoles at the center of each circular hole. Based on the addition theorem, it is transformed into the same coordinate centered at the center of one circle, where the boundary conditions are given. By matching the known boundary conditions, a coupled infinite system of simultaneous linear algebraic equations is obtained and then the scattered field can be determined according to the given incident flexural wave. Once the total field is calculated as the sum of the incident field and the scattered field, the dynamic moment concentration factor along the circular holes can be determined. Some numerical results of an infinite thin plate with three circular holes subject the incident flexural wave are presented. The effects of both the space among holes and the incident wave number on the DMCF are examined in this paper.

2. Problem statement of scattering of flexural wave

An infinite thin plate with H nonoverlapping circular holes subjected to the incident flexural wave is shown in Fig. 1, where $H+1$ observer coordinate systems are used: (x_1, x_2) is a global plane Cartesian coordinate centered at O, $(\rho_p,\ \phi_p)$ are H local plane polar coordinates centered at $O_p, p = 1, \ldots, H$. The radius of the pth circular hole is denoted by R_p and B_p is its corresponding boundary. The governing equation of motion for the transverse displacement $W(\boldsymbol{x},\ t)$ in a thin plate is

$$\rho_0 h \frac{\partial^2 W(\boldsymbol{x},\ t)}{\partial t^2} = -D\nabla^4 W(\boldsymbol{x},\ t) + Q, \quad \boldsymbol{x} \in \Omega^e, \tag{1}$$

where $\boldsymbol{x}$ is the field point, Ω^e is the unbounded exterior region occupied by the infinite plate, ∇^4 is the biharmonic operator, ρ_0 is the volume density, h is the plate thickness, $D = Eh^3/12(1-\mu^2)$ is the flexural rigidity of the plate, E denotes the Young's modulus, μ is the Poisson's ratio and Q is the external transverse load per unit area.

For $Q = 0$ and time-harmonic motion exclusively, solution of Eq. (1) is given by

$$W(\boldsymbol{x}, t) = w(\boldsymbol{x})e^{-i\omega t}, \tag{2}$$

where ω is the radian frequency. Hence the complex-valued function $w(\boldsymbol{x})$ satisfies the BiHelmholtz equation,

$$\nabla^4 w(\boldsymbol{x}) - k^4 w(\boldsymbol{x}) = 0, \tag{3}$$

where $k^4 = \omega^2\rho_0 h/D$ and k is the wave number.

The solution of Eq. (3) in the plane polar coordinates can be represented as

$$w(\rho, \phi) = w_1(\rho, \phi) + w_2(\rho, \phi), \tag{4}$$

where $w_1(\rho, \phi)$ and $w_2(\rho, \phi)$ are solutions of the following equations, respectively,

$$\nabla^2 w_1(\rho, \phi) + \lambda^2 w_1(\rho, \phi) = 0, \tag{5}$$

$$\nabla^2 w_2(\rho, \phi) - \lambda^2 w_2(\rho, \phi) = 0. \tag{6}$$

Eqs. (5) and (6) are the so-called Helmholtz equation and the modified Helmholtz equation, respectively. From solutions of Eqs. (5) and (6), the solution of Eq. (3) is explicitly expressed in series form as follows:

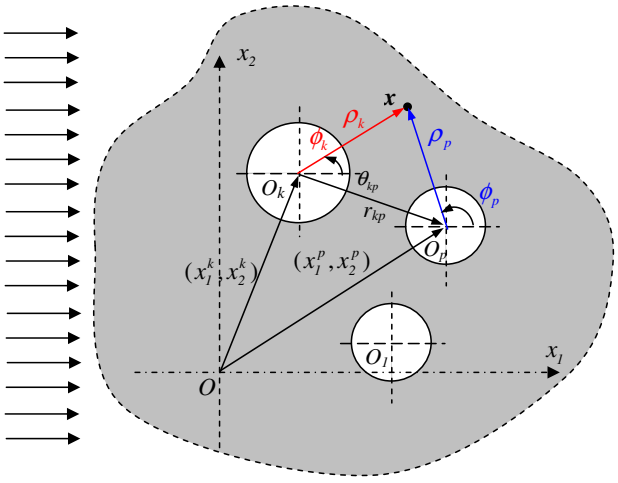

Fig. 1. Problem statement for an infinite plate with multiple circular holes subject to an incident flexural wave.

$$w(\rho,\phi)=\sum_{m=-\infty}^{\infty}\tilde{w}_m(\rho)e^{im\phi}, \tag{7}$$

where $\tilde{w}_m(\rho)$ is defined by

$$\tilde{w}_m(\rho)=c_m^1J_m(\lambda\rho)+c_m^2Y_m(\lambda\rho)+c_m^3I_m(\lambda\rho)+c_m^4K_m(\lambda\rho), \tag{8}$$

in which c_m^i $(i=1-4)$ are the coefficients, J_m and Y_m are the mth order Bessel functions; and I_m and K_m are the mth order modified Bessel functions. Based on the characteristics of functions at $\rho=0$ function and $\rho\to\infty$, the appropriate Bessel function and the modified Bessel are chosen to represent the transverse displacement field for the plate.

The w_1 in Eq. (5) represents the part of the flexural wave that travel in the plate and w_2 represents the part attenuating (Pao and Mow, 1972). When harmonic forces are applied perpendicularly to a thin plate, both parts of the flexural wave are excited. If the scatterer, such as a hole, is located at a great distance from the load, the displacement w_2 can be negligible due to attenuation and only the displacement w_1 need to be concerned as the incident flexural wave. Consequently, an incident flexural wave with an incident angle α with respect to the x_1 axis is represented by

$$W^{(i)}(\boldsymbol{x},t)=w_1(\boldsymbol{x})e^{-i\omega t}=w_0e^{i[(x_1\cos\alpha+x_2\sin\alpha)k-\omega t]}, \tag{9}$$

where w_0 is the amplitude of incident wave. By substituting $x_1=x_1^p+\rho_p\cos(\phi_p)$ and $x_2=x_2^p+\rho_p\sin(\phi_p)$ into Eq. (9) and omitting the time factor $e^{-i\omega t}$, the incident flexural wave in the pth circular hole is given by

$$w^{(i)}(\rho_p,\phi_p)=w_0c_pe^{ik\rho_p\cos(\phi_p-\alpha)},\quad p=1,\ldots,H, \tag{10}$$

where $c_p=e^{ik(x_1^p\cos\alpha+x_2^p\sin\alpha)}$ is a phase factor associated with the pth circular hole (Linton and Evans, 1990). From the Jacobi's expansion (Watson, 1995), $e^{ix\cos\phi}=\sum_{m=-\infty}^{\infty}i^mJ_m(x)e^{im\phi}$, Eq. (10) can be expanded in a series form

$$w^{(i)}(\rho_p,\phi_p)=\sum_{m=-\infty}^{\infty}a_m^{(i)}(k\rho_p)e^{im\phi_p},\quad p=1,\ldots,H, \tag{11}$$

where $a_m^{(i)}(k\rho_p)=c_pi^mJ_m(k\rho_p)e^{-im\alpha}$.

Based on the displacement field, the normal bending moment, tangential bending moment and effective shear force can be derived by applying the following three operators with respect to the field point,

$$m_n(\rho,\phi)=-D\left[\mu\nabla^2w(\rho,\phi)+(1-\mu)\frac{\partial^2w(\rho,\phi)}{\partial\rho^2}\right], \tag{12}$$

$$m_t(\rho,\phi)=-D\left[\nabla^2w(\rho,\phi)+(\mu-1)\frac{\partial^2w(\rho,\phi)}{\partial\rho^2}\right], \tag{13}$$

$$v(\rho,\phi)=-D\left[\frac{\partial}{\partial\rho}(\nabla^2w(\rho,\phi))+(1-\mu)\left(\frac{1}{\rho}\right)\frac{\partial}{\partial\phi}\left[\frac{\partial}{\partial\rho}\left(\frac{1}{\rho}\frac{\partial w(\rho,\phi)}{\partial\phi}\right)\right]\right]. \tag{14}$$

3. Analytical derivations for flexural wave scattered by multiple circular holes in a thin plate

Assume that a time harmonic incident flexural wave impinges on an infinite thin plate containing H circular holes as shown in Fig. 1. The problem of flexural wave scattered by H circular holes is to solve Eq. (3) subject to the free traction along each circular edge and a radiation condition at infinity, i.e. the scattered field equaling to zero when $\rho\to\infty$. Based on Eq. (7), we can express the scattered field as an infinite sum of multipoles at the center of each hole as follows:

$$w^{(sc)}(\boldsymbol{x};\ \rho_1,\ \phi_1,\ldots,\ \rho_H,\ \phi_H)=\sum_{k=1}^{H}\left[\sum_{m=-\infty}^{\infty}a_m^kH_m^{(1)}(k\rho_k)e^{im\phi_k}+b_m^kK_m(k\rho_k)e^{im\phi_k}\right], \tag{15}$$

where $(\rho_1,\phi_1),\ldots,(\rho_H,\varphi_H)$ are the polar coordinates of the field point $\boldsymbol{x}$ with respect to each center of holes. The Hankel function $(J+iY)$ and the modified Bessel function K are chosen to represent the infinite plate due to their values being finite as $\rho\to\infty$. The coefficients of a_m^k and b_m^k, $k=1,\ldots,H;m=0,\pm1,\pm2,\ldots$, are determined by matching the boundary condition on each circle. To satisfy the specified boundary conditions, the total field is required and defined by

$$w(\boldsymbol{x})=w^{(i)}(\boldsymbol{x})+w^{(sc)}(\boldsymbol{x}). \tag{16}$$

By combining Eqs. (11) and (15), the total field is explicitly represented by

$$w(\boldsymbol{x};\ \rho_1,\ \phi_1,\ldots,\ \rho_H,\ \phi_H)=\sum_{m=-\infty}^{\infty}a_m^{(i)}(k\rho_p)e^{im\phi_p}+\sum_{k=1}^{H}\left[\sum_{m=-\infty}^{\infty}a_m^kH_m^{(1)}(k\rho_k)e^{im\phi_k}+b_m^kK_m(k\rho_k)e^{im\phi_k}\right],\quad p=1,\ldots,H. \tag{17}$$

In the following, we are mainly concerned with the free traction condition for each circular edge. The bending moment and shear force along each hole, $p=1,\ldots,H$, can be obtained by substituting Eq. (17) into Eqs. (12) and (14). The unknown coefficients of a_m^k and b_m^k can be determined through the following boundary conditions.

$$m_n(\rho_p,\phi_p)=0,\quad \rho_p=R_p,\quad 0\leqslant\phi_p\leqslant2\pi,\quad p=1,\ldots,H, \tag{18}$$

$$v(\rho_p,\phi_p)=0,\quad \rho_p=R_p,\quad 0\leqslant\phi_p\leqslant2\pi,\quad p=1,\ldots,H. \tag{19}$$

But it is difficult to determine the unknown coefficients by using the procedure mentioned above. This question can be answered by applying the addition theorem (Watson, 1995) which will be described in the following.

Based on the Graf's addition theorem for the Bessel functions, we can express the theorem in the following form,

$$J_m(k\rho_k)e^{im\phi_k}=\sum_{n=-\infty}^{\infty}J_{m-n}(kr_{kp})e^{i(m-n)\theta_{kp}}J_n(k\rho_p)e^{in\phi_p}, \tag{20}$$

$$I_m(k\rho_k)e^{im\phi_k}=\sum_{n=-\infty}^{\infty}I_{m-n}(kr_{kp})e^{i(m-n)\theta_{kp}}I_n(k\rho_p)e^{in\phi_p}, \tag{21}$$

$$H_m^{(1)}(k\rho_k)e^{im\phi_k}=\begin{cases}\sum_{n=-\infty}^{\infty}H_{m-n}^{(1)}(kr_{kp})e^{i(m-n)\theta_{kp}}J_n(k\rho_p)e^{in\phi_p}, & \rho_p<r_{kp},\\ \sum_{n=-\infty}^{\infty}J_{m-n}(kr_{kp})e^{i(m-n)\theta_{kp}}H_n^{(1)}(k\rho_p)e^{in\phi_p}, & \rho_p>r_{kp},\end{cases} \tag{22}$$

$$K_m(k\rho_k)e^{im\phi_k}=\begin{cases}\sum_{n=-\infty}^{\infty}(-1)^nK_{m-n}(kr_{kp})e^{i(m-n)\theta_{kp}}I_n(k\rho_p)e^{in\phi_p}, & \rho_p<r_{kp},\\ \sum_{n=-\infty}^{\infty}(-1)^{m-n}I_{m-n}(kr_{kp})e^{i(m-n)\theta_{kp}}K_n(k\rho_p)e^{in\phi_p}, & \rho_p>r_{kp},\end{cases} \tag{23}$$

where (ρ_p,φ_p) and (ρ_k,φ_k) as shown in Fig. 1 are the polar coordinates of the field point $\boldsymbol{x}$ with respect to O_p and O_k, respectively, which are the origins of two polar coordinate systems and (r_{kp},θ_{kp}) are the polar coordinates of O_p with respect to O_k.

By substituting the addition theorem for the Bessel functions $H_m^{(1)}(k\rho_k)$ and $K_m(k\rho_k)$ into Eq. (17), the displacement field near the circular boundary B_p for the case of $\rho_p < r_{kp}$ is given by

$$w(\boldsymbol{x};\rho_p,\phi_p) = \sum_{m=-\infty}^{\infty} a_m^{(i)}(k\rho_p)e^{im\phi_p} + \left[\sum_{m=-\infty}^{\infty} a_m^p H_m^{(1)}(k\rho_p) + \sum_{m=-\infty}^{\infty} b_m^p K_m(k\rho_p)\right]e^{im\phi_p} + \sum_{\substack{k=1\\k\neq p}}^{H}\left[\sum_{m=-\infty}^{\infty} a_m^k \sum_{n=-\infty}^{\infty} H_{m-n}^{(1)}(kr_{kp})e^{i(m-n)\theta_{kp}}J_n(k\rho_p) + b_m^k \sum_{n=-\infty}^{\infty}(-1)^n K_{m-n}(kr_{kp})e^{i(m-n)\theta_{kp}}I_n(k\rho_p)\right]e^{in\phi_p}. \tag{24}$$

Furthermore, Eq. (24) can be rewritten as

$$w(\boldsymbol{x};\rho_p,\phi_p) = \sum_{m=-\infty}^{\infty} e^{im\phi_p}\left\{a_m^{(i)}(k\rho_p) + H_m^{(1)}(k\rho_p)a_m^p + K_m(k\rho_p)b_m^p + \sum_{\substack{k=1\\k\neq p}}^{H}\left[\sum_{n=-\infty}^{\infty} A_{mn}^k(k\rho_p)a_n^k + B_{mn}^k(k\rho_p)b_n^k\right]\right\}, \tag{25}$$

where

$$A_{mn}^k(k\rho_p) = H_{n-m}^{(1)}(kr_{kp})e^{i(n-m)\theta_{kp}}J_m(k\rho_p), \tag{26}$$

$$B_{mn}^k(k\rho_p) = (-1)^m e^{i(n-m)\theta_{kp}}K_{n-m}(kr_{kp})I_m(k\rho_p). \tag{27}$$

By substituting Eq. (25) into Eq. (12), the normal bending moment, $m_n(x)$, near the circular boundary $B_p(p = 1,\ldots,H)$ is given by

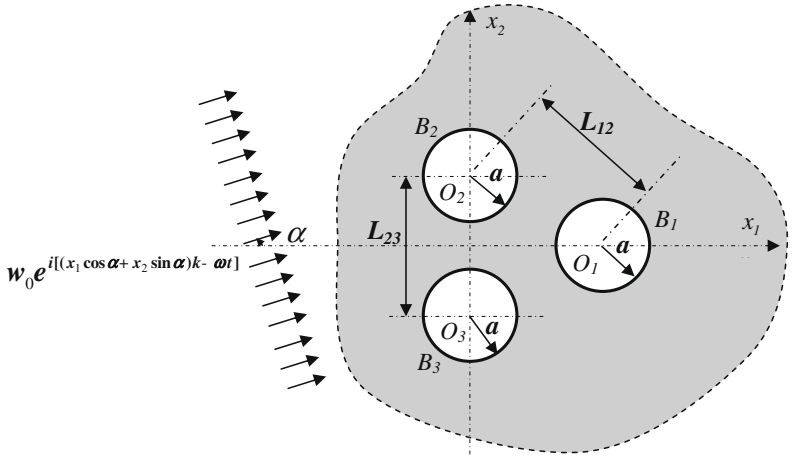

Fig. 2. An infinite thin plate with three circular holes subject to an incident flexural wave.

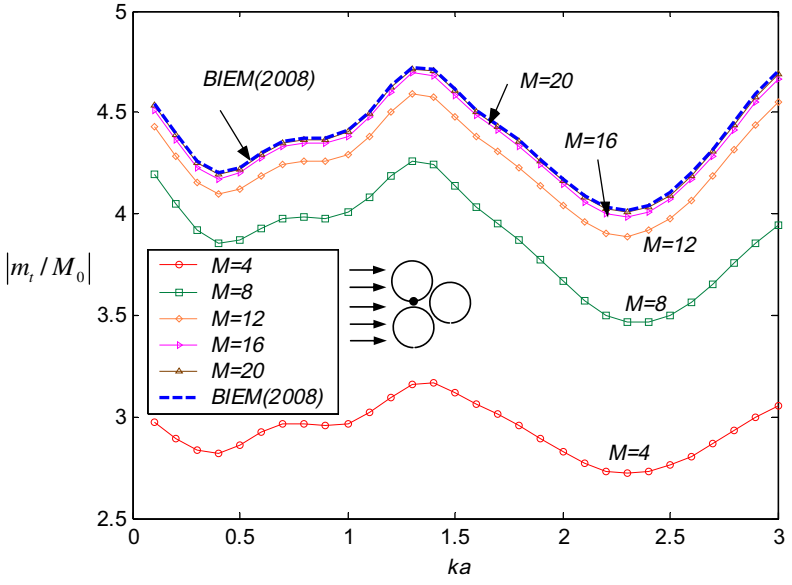

Fig. 3. DMCF on the second circular boundary $B_2(\theta = -\pi/2)$ versus the dimensionless wave number by using different truncated number of coefficients ($L_{12}/a = 2.1$ and $L_{23}/a = 2.1$).

$$m_n(\boldsymbol{x};\rho_p,\ \phi_p) = \sum_{m=-\infty}^{\infty} e^{im\phi_p}\left\{c_m^{(i)}(k\rho_p) + \alpha_m^H(k\rho_p)a_m^p + \alpha_m^K(k\rho_p)b_m^p + \sum_{\substack{k=1\\k\neq p}}^{H}\left[\sum_{n=-\infty}^{\infty} C_{mn}^k(k\rho_p)a_n^k + D_{mn}^k(k\rho_p)b_n^k\right]\right\}, \tag{28}$$

where

$$C_{mn}^k(k\rho_p) = H_{n-m}^{(1)}(kr_{kp})e^{i(n-m)\theta_{kp}}\alpha_m^J(k\rho_p), \tag{29}$$

$$D_{mn}^k(k\rho_p) = (-1)^m e^{i(n-m)\theta_{kp}}K_{n-m}(kr_{kp})\alpha_m^I(k\rho_p), \tag{30}$$

$$c_m^{(i)}(k\rho_p) = c_p i^m \alpha_m^J(k\rho_p)e^{-im\alpha}. \tag{31}$$

The moment operator $\alpha_m^X(k\rho)$ from Eq. (12) is defined as

$$\alpha_m^X(k\rho) = D\left\{(1-\mu)\frac{X_m'(k\rho)}{\rho} - \left[(1-\mu)\frac{m^2}{\rho^2} \mp k^2\right]X_m(k\rho)\right\}, \tag{32}$$

where the upper (lower) signs refer to $X = J, Y, H, (I, K)$, respectively. The second order differential equations for these functions have been used to simplify $\alpha_m^X(k\rho)$.

Similarly, the effective shear operator $\beta_m^X(k\rho)$ derived from Eq. (14) can be expressed as,

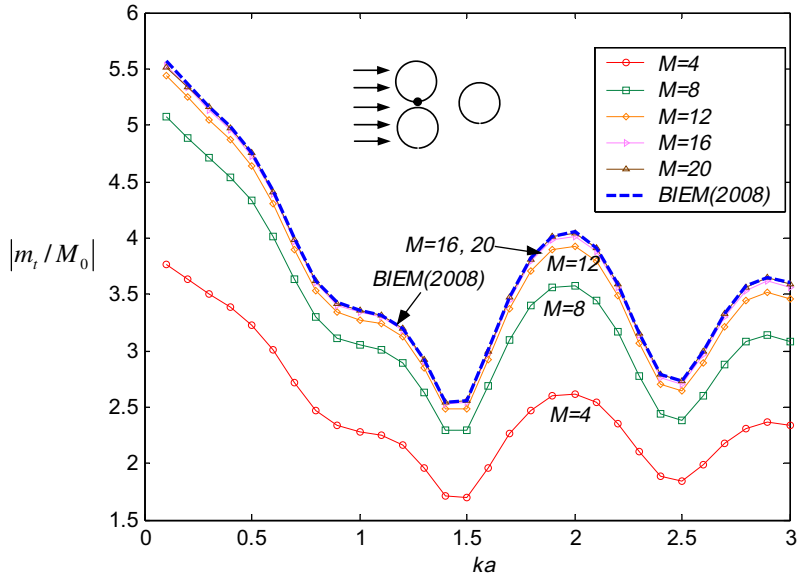

Fig. 4. DMCF on the second circular boundary $B_2(\theta = -\pi/2)$ versus the dimensionless wave number by using different truncated number of coefficients ($L_{12}/a = 4.0$ and $L_{23}/a = 2.1$).

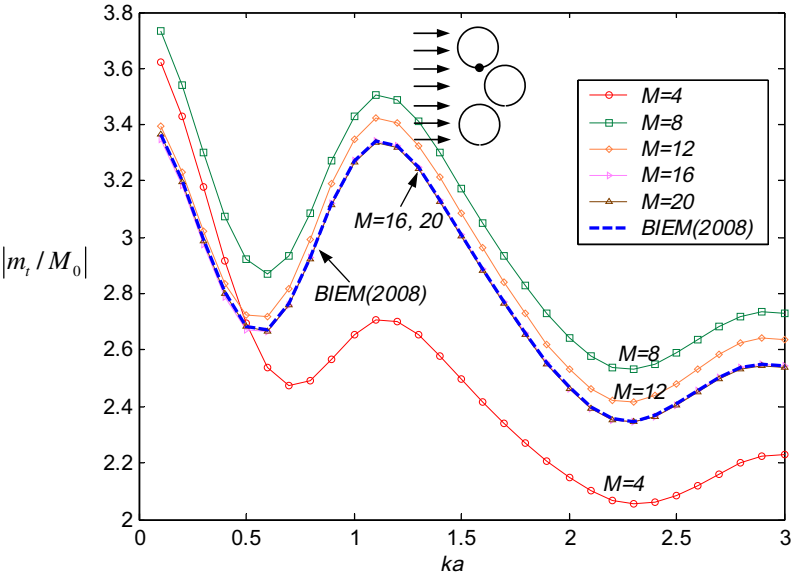

Fig. 5. DMCF on the second circular boundary $B_2(\theta = -\pi/2)$ versus the dimensionless wave number by using different truncated number of coefficients ($L_{12}/a = 2.1$ and $L_{23}/a = 4.0$).

$$\beta_m^X(k\rho) = D\left\{\left[m^2(1-\mu) \pm (k\rho)^2\right]\frac{X_m'(k\rho)}{\rho^2} - m^2(1-\mu)\frac{X_m(k\rho)}{\rho^3}\right\}, \tag{33}$$

and the field of effective shear, $v(x)$, near the circular boundary $B_p (p = 1, \ldots, H)$ is given by

$$v(\boldsymbol{x}; \rho_p, \phi_p) = \sum_{m=-\infty}^{\infty} e^{im\phi_p}\left\{d_m^{(i)}(k\rho_p) + \beta_m^H(k\rho_p)a_m^p + \beta_m^K(k\rho_p)b_m^p + \sum_{\substack{k=1\\k\neq p}}^{H}\left[\sum_{n=-\infty}^{\infty} E_{mn}^k(k\rho_p)a_n^k + F_{mn}^k(k\rho_p)b_n^k\right]\right\}, \tag{34}$$

where $E_{mn}^k(k\rho_p), F_{mn}^k(k\rho_p)$ and $d_m^{(i)}(k\rho_p)$ are obtained by replacing $\alpha_m^X(k\rho_p)$ in Eqs. (29)–(31) with $\beta_m^X(k\rho_p)$, respectively.

Based on the traction-free conditions of Eqs. (18) and (19), applying the orthogonal property of $\{e^{im\phi_p}\}$ to Eqs. (28) and (34), respectively, gives

$$\begin{cases} \alpha_m^H(kR_p)a_m^p + \alpha_m^K(kR_p)b_m^p + \sum\limits_{\substack{k=1\\k\neq p}}^{H}\left[\sum\limits_{n=-\infty}^{\infty} C_{mn}^k(kR_p)a_n^k + D_{mn}^k(kR_p)b_n^k\right] = -c_m^{(i)}(kR_p) \\ \beta_m^H(kR_p)a_m^p + \beta_m^K(kR_p)b_m^p + \sum\limits_{\substack{k=1\\k\neq p}}^{H}\left[\sum\limits_{n=-\infty}^{\infty} E_{mn}^k(kR_p)a_n^k + F_{mn}^k(kR_p)b_n^k\right] = -d_m^{(i)}(kR_p) \end{cases}, \tag{35}$$

for $m = 0, \pm1, \pm2, \ldots, n = 0, \pm1, \pm2, \ldots$, and $p = 1, \ldots, H$. Eq. (35) is a coupled infinite system of simultaneous linear algebraic equations which is the analytical model for the flexural scattering of an infinite plate containing multiple holes. In order to evaluate the numerical results in the following section, the infinite system of Eq. (35) is

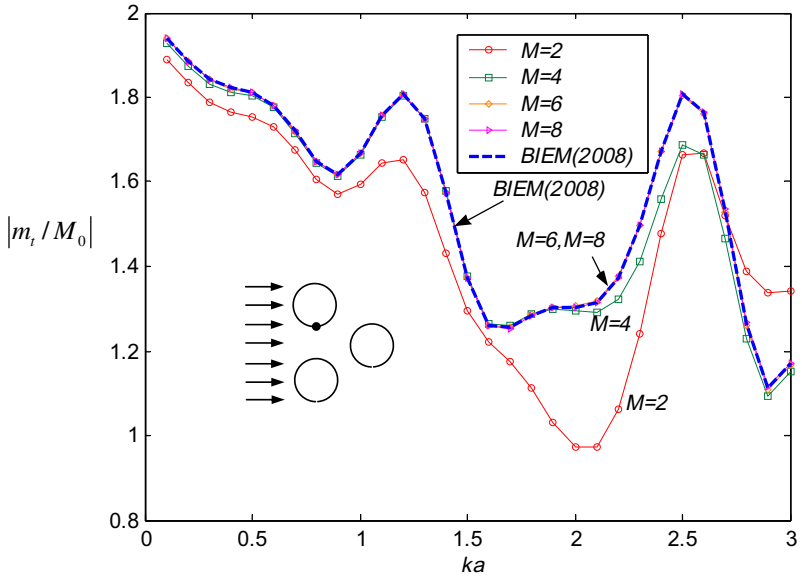

Fig. 6. DMCF on the second circular boundary $B_2(\theta = -\pi/2)$ versus the dimensionless wave number by using different truncated number of coefficients ($L_{12}/a = 4.0$ and $L_{23}/a = 4.0$).

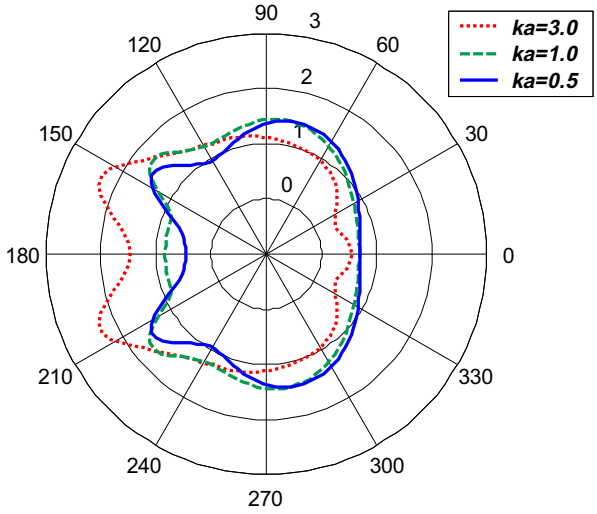

Fig. 7. Distribution of DMCF on the first circular boundary B_1 at three different dimensionless wave numbers, solid line for $ka = 0.5$, dashed line for $ka = 1.0$ and dotted line for $ka = 3.0$ ($L/a = 2.1$).

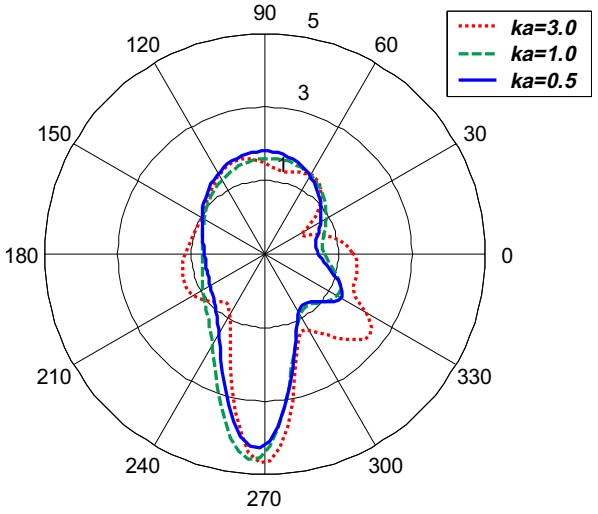

Fig. 8. Distribution of DMCF on the second circular boundary B_2 at three different dimensionless wave numbers, solid line for $ka = 0.5$, dashed line for $ka = 1.0$ and dotted line for $ka = 3.0$ ($L/a = 2.1$).

truncated to a $(2H)(2M+1)$ system of equations for $(2H)(2M+1)$ unknown coefficients, i.e. $m = 0, \pm1, \pm2, \ldots, \pm M$. Once the coefficients a_m^k and $b_m^k (k = 1, \ldots, H; m = 0, \pm1, \pm2, \ldots, \pm M)$ are determined, the total field of displacement, the bending moment and the shear force can be obtained by substituting them into Eqs. (17), (28) and (34).

In the polar coordinates, the normal bending moment, tangential bending moment and effective shear force induced by the incident wave can be determined by substituting Eq. (10) into Eqs. (12)–(14). By setting the amplitude of incident wave to be one $(w_0 = 1)$, the amplitude of normal bending moment produced by the incident wave is

$$M_0 = Dk^2. \tag{36}$$

The dynamic moment concentration factor (DMCF) at any field point $\boldsymbol{x}$ is defined as

$$\mathrm{DMCF}(\boldsymbol{x}) = m_t(\boldsymbol{x})/M_0, \tag{37}$$

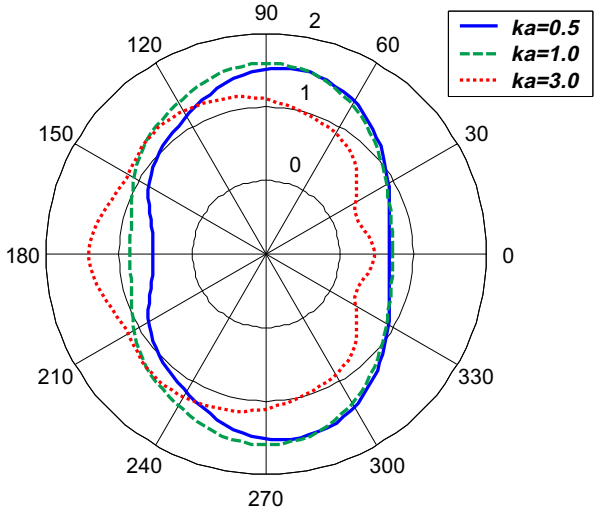

Fig. 9. Distribution of DMCF on the first circular boundary B_1 at three different dimensionless wave numbers, solid line for $ka = 0.5$, dashed line for $ka = 1.0$ and dotted line for $ka = 3.0$ $(L/a = 2.5)$.

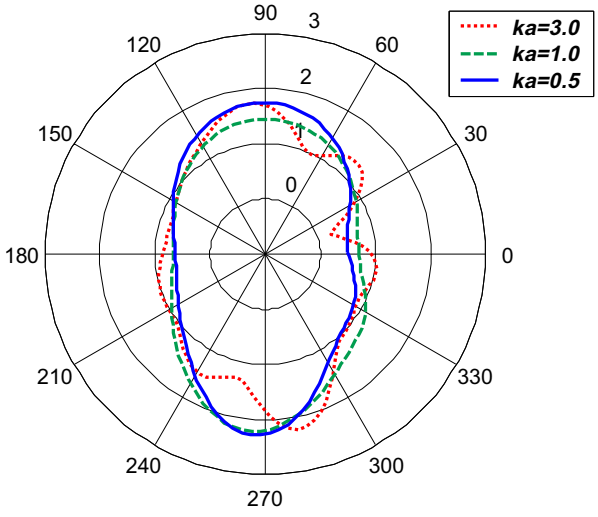

Fig. 10. Distribution of DMCF on the second circular boundary B_2 at three different dimensionless wave numbers, solid line for $ka = 0.5$, dashed line for $ka = 1.0$ and dotted line for $ka = 3.0$ $(L/a = 2.5)$.

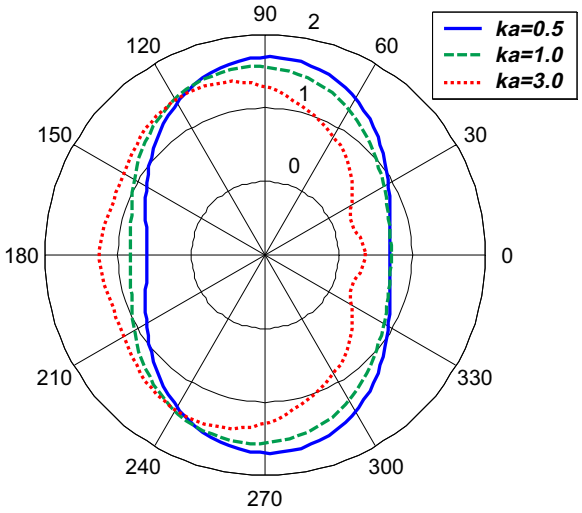

Fig. 11. Distribution of DMCF on the first circular boundary B_1 at three different dimensionless wave numbers, solid line for $ka = 0.5$, dashed line for $ka = 1.0$ and dotted line for $ka = 3.0$ $(L/a = 4.0)$.

where the tangential bending moment $m_t(x)$ is determined by substituting Eq. (25) into Eq. (13) with respective to the field point.

$$m_t(\boldsymbol{x}; \rho_p, \phi_p) = \sum_{m=-\infty}^{\infty} e^{im\phi_p} \left\{ f_m^{(i)}(k\rho_p) + \gamma_m^H(k\rho_p) a_m^p + \gamma_m^K(k\rho_p) b_m^p + \sum_{\substack{k=1 \\ k\neq p}}^{H} \left[\sum_{n=-\infty}^{\infty} G_{mn}^k(k\rho_p) a_n^k + H_{mn}^k(k\rho_p) b_n^k \right] \right\}, \tag{38}$$

where $G_{mn}^k(k\rho_p), H_{mn}^k(k\rho_p)$ and $f_m^{(i)}(k\rho_p)$ are obtained by replacing $\alpha_m^X(k\rho_p)$ in Eqs. (29)–(31) with $\gamma_m^X(k\rho_p)$, respectively, and the tangential bending moment operator $\gamma_m^X(k\rho)$ derived from Eq. (13) is given by

$$\gamma_m^X(k\rho) = D\left\{ (\mu - 1)\frac{X_m'(k\rho)}{\rho} - \left[(\mu - 1)\frac{m^2}{\rho^2} \mp \mu k^2 \right] X_m(k\rho) \right\}. \tag{39}$$

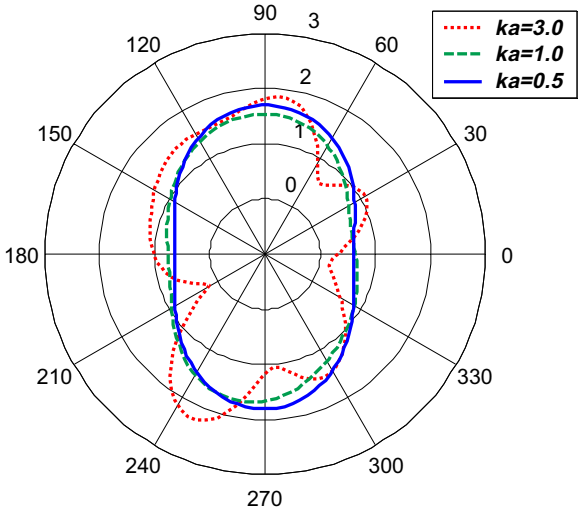

Fig. 12. Distribution of DMCF on the second circular boundary B_2 at three different dimensionless wave numbers, solid line for $ka = 0.5$, dashed line for $ka = 1.0$ and dotted line for $ka = 3.0$ $(L/a = 4.0)$.

4. Numerical results and discussions

To demonstrate the validity of the proposed method, the FORTRAN code was implemented to solve the flexural wave scattered by three circular holes which are symmetric about the x_1-axis in an infinite thin plate as shown in Fig. 2, where L_{12} denotes the central distances of the first hole and the second hole; L_{23} is that of the second hole and the third hole. The notation L stands for the central distances between holes when their separation distances are equal to each other. The coordinates of three holes are $(\sqrt{L_{12}^2-(L_{23}/2)^2},0),(0,L_{23}/2)$ and $(0,-L_{23}/2)$, respectively. The DMCF around the circular hole is determined since it is important to the structure design such as fatigue failure evaluation. In all cases, all edges of holes are subjected to the traction-free boundary condition and the thickness of plate is 0.002 m.

Fig. 3 show DMCF on the second circular boundary B_2 $(\theta=-\pi/2)$ versus the dimensionless wave number by using different truncated number of coefficients when $L_{12}/a=2.1$ and $L_{23}/a=2.1$. It can be seen that the convergence is fast achieved as the truncated number M increases. The proposed results with M=20 match well with the convergent results provided by BIEM (Lee and Chen, 2008) in which thirty terms of Fourier series are used. Moreover, during the convergence, fictitious frequency appearing in BIEM (Lee and Chen, 2008) does not appear in the multipole Trefftz method. In the convergence analysis, the maximum of the allowable truncated number M is limited by the minimum value of ka considered, for instance here ka=0.1. The reason

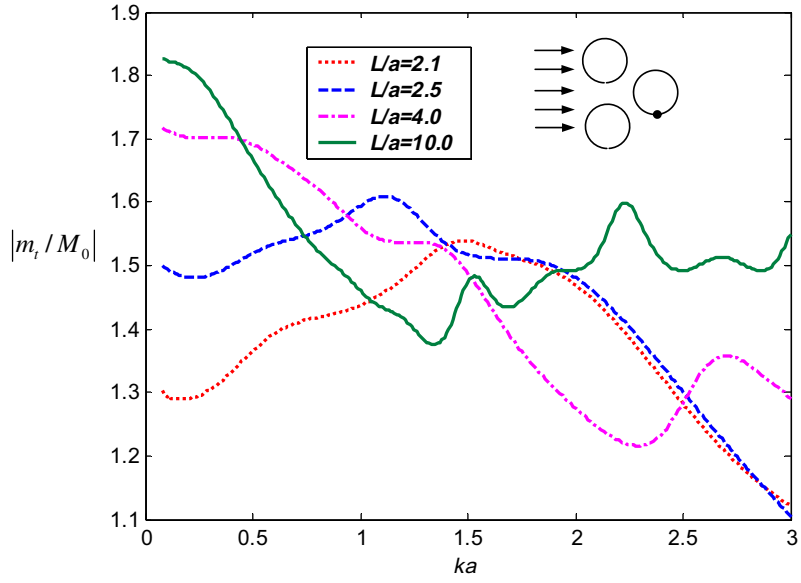

Fig. 13. DMCF on the first circular boundary $B_1(\phi=-\pi/2)$ versus the dimensionless wave number at four different dimensionless central distances, dotted line for L/a = 2.1, dashed line for L/a = 2.5, dot-dashed line for L/a = 4.0 and solid line for L/a = 10.0.

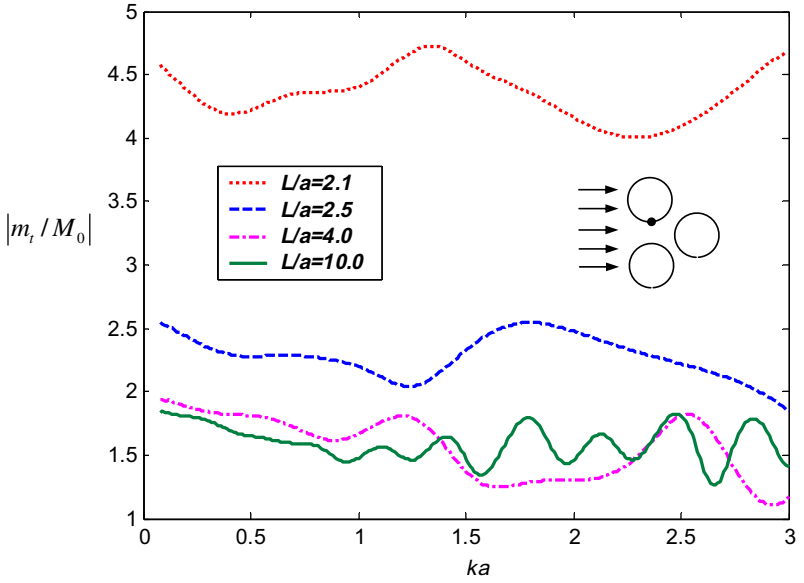

Fig. 14. DMCF on the second circular boundary B_2 $(\phi=-\pi/2)$ versus the dimensionless wave number at four different dimensionless central distances, dotted line for L/a = 2.1, dashed line for L/a = 2.5, dot-dashed line for L/a = 4.0 and solid line for L/a = 10.0.

for this is that the Bessel functions of $Y_m(kR_p)$ and $I_m(kR_p)$ of Eq. (35) become large when k is small. Actually, the truncated number M can increase while the concerned minimum value of ka increases.

The convergence analyses for the case of the multiple holes with different separation distances are shown in Figs. 4 and 5. When $L_{12}/a = 4.0$ and $L_{23}/a = 2.1$, that is, one of the separation distances become large, the convergent rate increases. Even though this, the required number of M is suggested to take twenty to consider the minimum separation distance. The other is the case of $L_{12}/a = 2.1$ and $L_{23}/a = 4.0$. The convergence rate is still fast but the approach to the convergence is from the upper rather than the lower. When $L_{12}/a = 4.0$ and $L_{23}/a = 4.0$ shown in Fig. 6, that is, both of the separation distances become large, the convergent rate significantly increases and then the required number of M can reduce to six or eight.

In summary, to obtain the more accurate results, numerical experiments show that the required number of M in the finite system mainly depends on the considered minimum dimensionless central distance L/a. Through the numerical experiments, it is found that the required number of M can be taken from 20 to 8 for the minimum separation distance L/a ranged from 2.1 to 10.0. Only when does the value of L/a become large such as 4.0 or 10.0, the required number of M is related to the incident wave number. In other words, the required number of M to converge increases as the incident wave number becomes larger.

Figs. 7–12 show the distribution of DMCF on the first and the second circular boundary B_1 and B_2, respectively, when three

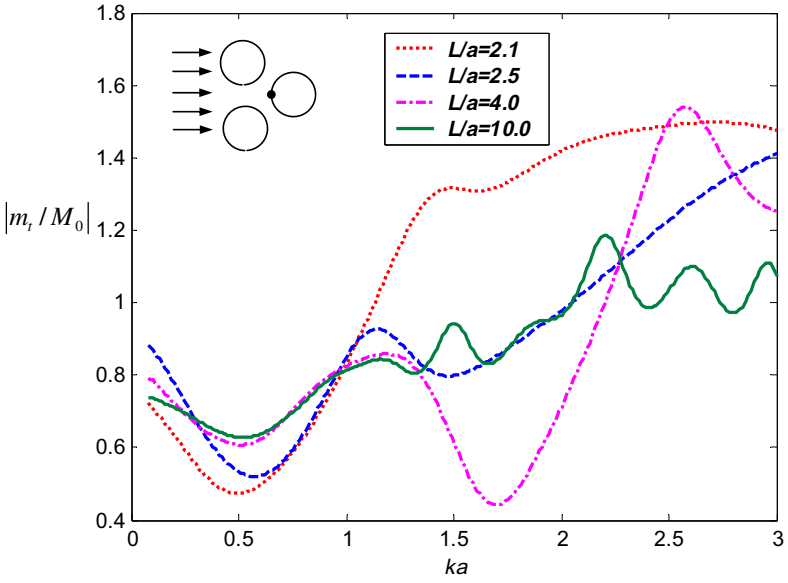

Fig. 15. DMCF on the first circular boundary $B_1(\phi = \pi)$ versus the dimensionless wave number at four different dimensionless central distances, dotted line for $L/a = 2.1$, dashed line for $L/a = 2.5$, dot-dashed line for $L/a = 4.0$ and solid line for $L/a = 10.0$.

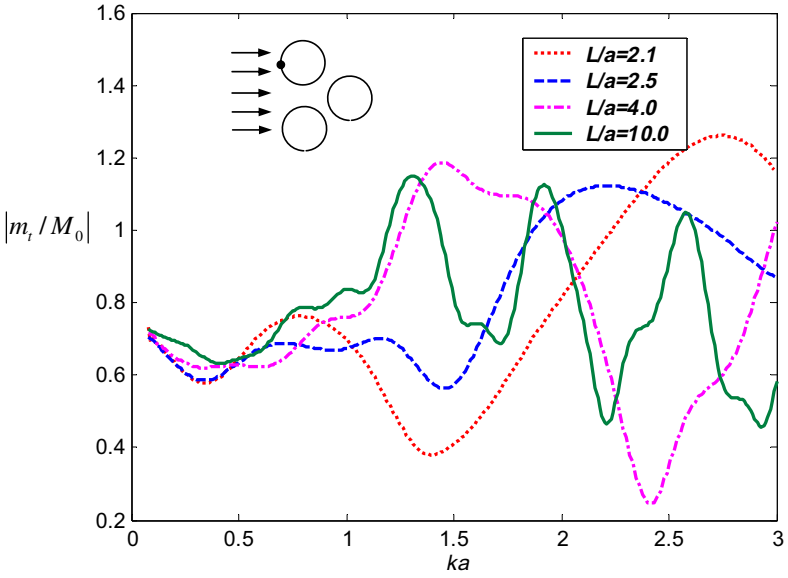

Fig. 16. DMCF on the second circular boundary $B_2(\phi = \pi)$ versus the dimensionless wave number at four different dimensionless central distances, dotted line for $L/a = 2.1$, dashed line for $L/a = 2.5$, dot-dashed line for $L/a = 4.0$ and solid line for $L/a = 10.0$.

different incident dimensionless wave numbers (ka=0.5, 1.0 and 3.0) and three different dimensionless central distance (L/a=2.1, 2.5 and 4.0) are considered. The distribution of DMCF on the third circular boundary B_3 is equal to that on the second one due to the symmetry of the x_1-axis, so that it is not presented here. It can be observed that the distribution of DMCF of three circular holes is different from that of one, where the maximum of DMCF occurs at $\phi = \pi/2$ and $-\pi/2$ when the incident wave number is small and the incident angle equals to zero.

In addition to the incident wave number, the distribution of DMCF apparently depends on two factors. One is the geometry and the other is the angle of the incident wave. Since the first circular hole is located near the other circular holes at $\phi = 5\pi/6$ and $-5\pi/6$ where the separated space is very small and meanwhile the incident wave is from the negative direction of the x_1 axis, the maximum of DMCF on the boundary of the first hole occurs at $\phi = \pi/2, 5\pi/6, -5\pi/6$ and $-\pi/2$ as shown in Fig. 7. As the value of ka increases, the factor of geometry is obviously amplified but that of incident angle is attenuated a little. Fig. 8 shows that the maximum of DMCF on the boundary of the second hole occurs at $\phi = -\pi/2$ and $-\pi/6$. The maximum of DMCF at $\phi = -\pi/6$ is similar to those of the first hole. But the maximum of DMCF at $\phi = -\pi/2$ is the largest of all considered so far because two factors simultaneously occur at this point: the narrow space and the incident flexural wave with α=0.

As the dimensionless central distance L/a increases to 2.5 and 4.0 as shown in Figs. 9–12, the DMCF gradually decreases since the geometry factor is attenuating. Meanwhile the shadow on the first hole coming from the other holes gradually decreases so that the more incident wave impinges on the first holes.

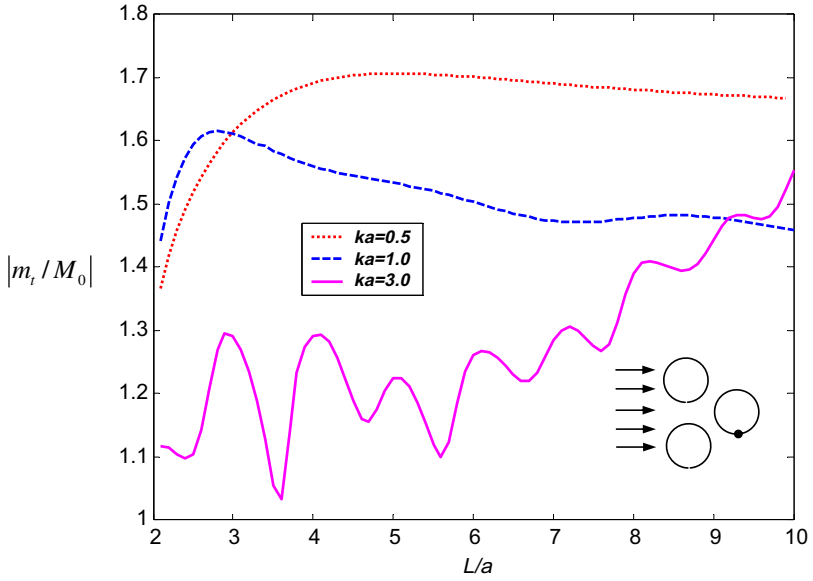

Fig. 17. DMCF on the first circular boundary $B_1(\phi = -\pi/2)$ versus the dimensionless central distance at three different dimensionless wave numbers, dotted line for ka = 0.5, dashed line for ka = 1.0 and solid line for ka = 3.0.

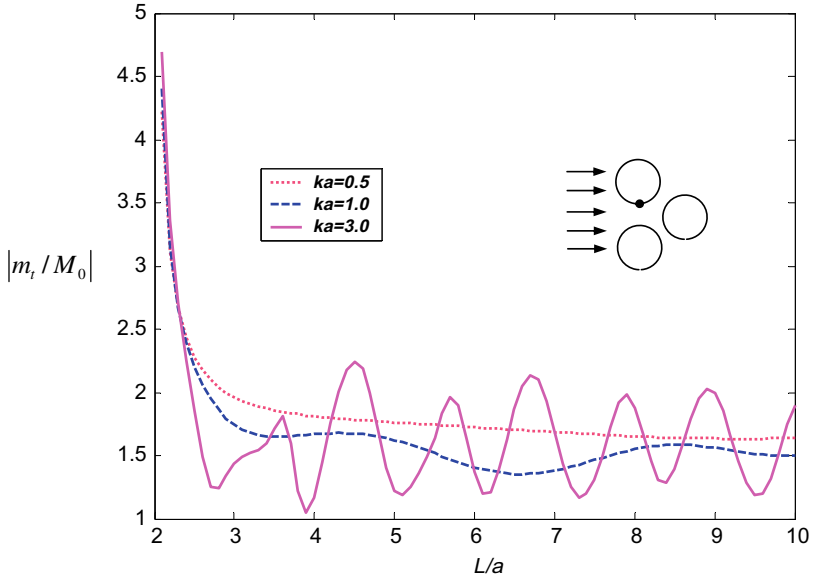

Fig. 18. DMCF on the second circular boundary $B_2(\phi = -\pi/2)$ versus the dimensionless central distance at three different dimensionless wave numbers, dotted line for ka = 0.5, dashed line for ka = 1.0 and solid line for ka = 3.0.

Accordingly, the magnitude of DMCF of the first hole at $\phi = \pi/2$ and $-\pi/2$ becomes large instead of decreasing as shown in Figs. 7, 9 and 11. As the dimensionless incident wave number increases, the tendency to change for the first hole is different from that for the second hole. The former is mainly backscattering with sidescattering attenuated and the latter shows obviously fluctuation along azimuthal coordinate.

Figs. 13–16 show DMCF on the first and the second circular boundaries at $\phi = -\pi/2$ and π as a function of the dimensionless incident wave number at four different dimensionless central distances, dotted line for L/a = 2.1, dashed line for L/a = 2.5, dot-dashed line for L/a = 4.0 and solid line for L/a = 10.0. It can be seen from Fig. 13 that the DMCF on the first circular boundary at $\phi = -\pi/2$ is apparently related to the space between holes when the incident wave number is small. Because of the shadow effect, the smaller the central distance is; the smaller the DMCF is. This effect is gradually replaced by that of the multiple scattering as the incident wave number ka increases. Instead of the incident wave number, the geometry factor dominates the DMCF on the second circular boundary at $\phi = -\pi/2$ as shown in Fig. 14. It can be seen that when space is large enough such as L/a=10.0 and ka approaches zero, the value of DMCF approaches 1.85 which agrees with the analytical solution of an infinite plate with one hole (Pao and Mow, 1972). From Figs. 15 and 16, the magnitude of DMCF on the first circular boundary at $\phi = \pi$ is larger than that on the second boundary instead of being small, since the effect of multiple scattering is greater than that of shadow. It can be seen that as the value of ka increases, the magnitude of DMCF along the ka becomes more fluctuated especially for the case of the large value of L/a.

Figs. 17–20 show DMCF on the first and the second circular boundaries at $\phi = -\pi/2$ and π as a function of the dimensionless central distance at three different dimensionless incident wave

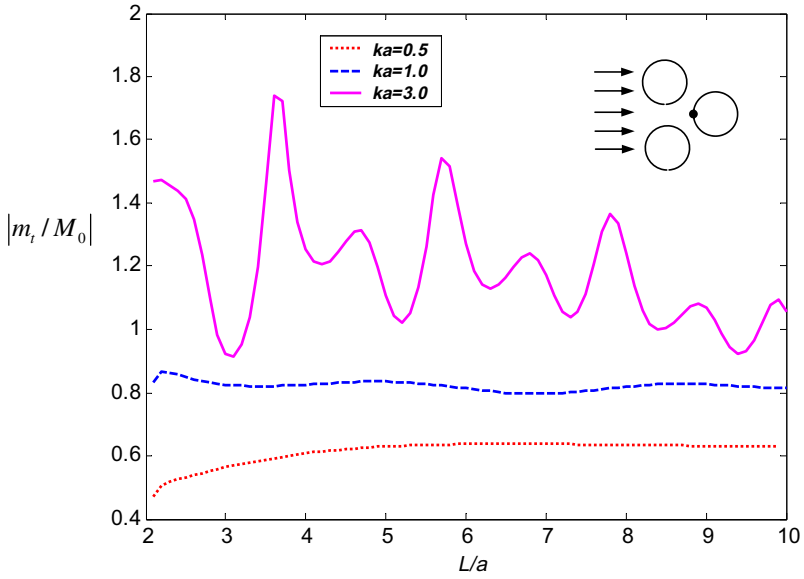

Fig. 19. DMCF on the first circular boundary $B_1(\phi = \pi)$ versus the dimensionless central distance at three different dimensionless wave numbers, dotted line for ka = 0.5, dashed line for ka = 1.0 and solid line for ka = 3.0.

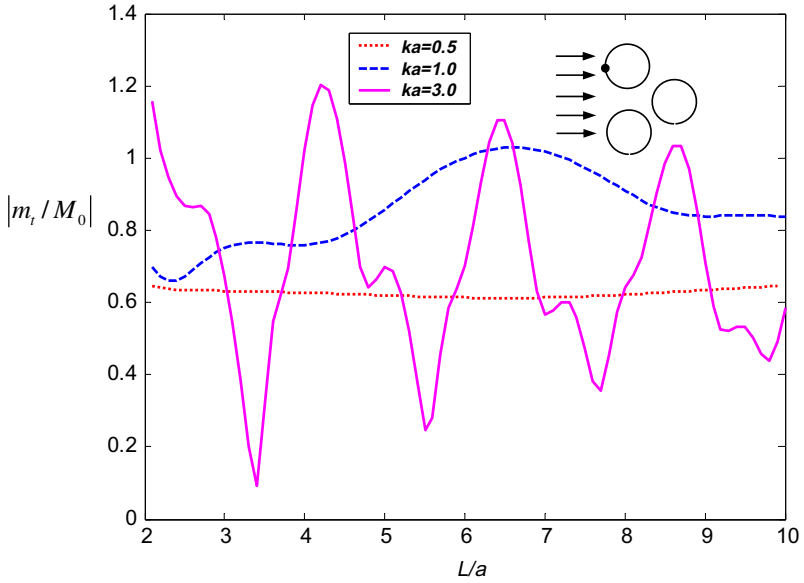

Fig. 20. DMCF on the second circular boundary $B_2(\phi = \pi)$ versus the dimensionless central distance at three different dimensionless wave numbers, dotted line for ka = 0.5, dashed line for ka = 1.0 and solid line for ka = 3.0.

numbers, dotted line for ka = 0.5, dashed line for ka = 1.0 and solid line for ka = 3.0. It can be seen from Fig. 17 that the shadow effect at the low incident wave number is rapidly released as the separation distance increases. Comparing Figs. 17 with 18, even though two plots varied in the different way, these variations will converge to the same level as the value of L/a approaches to infinite. From Figs. 19 and 20, the magnitude of DMCF on the first circular boundary at $\phi = \pi$ is also larger than that on the second boundary. It can be seen from Figs. 17–20 that for the high incident wave number the DMCF shows obvious oscillation as the space among holes varies. Actually, this oscillation exits in all cases of the incident wave number and the detail can be seen in the recent paper of Lee and Chen (2008).

5. Concluding remarks

The flexural wave scattered by multiple circular holes in a thin plate has been theoretically solved by using the multipole Trefftz method. With the aid of the addition theorem, the Trefftz method can be extended to deal with multiply-connected domain problems. The proposed algorithm is general and easily applicable to problems with multiple holes which are not easily solved by using the traditional analytical method. By matching boundary conditions, the analytical model for the multiple scattering of the plate problem is derived as a coupled infinite system of simultaneous equations in which the coefficients can be determined simultaneously rather than recessively. The convergence analysis was implemented and gave some guidelines on the selection of the truncation limit in the numerical computation. An example of an infinite plate containing three holes in a truncated system is presented and the effects of the central distance and the incident wave number on the dynamic moment concentration factor (DMCF) are investigated in this paper. The distribution of DMCF of three holes is significantly different that of one. The geometry factor mainly affects the distribution of DMCF, especially under the specified direction of incident wave.

Acknowledgements

Financial support from the National Science Council under the Grant No. NSC-98-2221-E-157-002 and NSC-98-2221-E-019-017-MY3 for China University of Science and Technology and National Taiwan Ocean University, respectively, is gratefully appreciated.

References

Fang, X.Q., Hu, C., Wang, D.B., 2008. Multiple scattering of flexural waves from two cutouts in a semi-infinite thin plate. International Journal of Solids and Structures 45, 4236–4246.

Gao, S.W., Wang, B.L., Ma, X.R., 2001. Scattering of elastic wave and dynamic stress concentrations in thin plate with a circular hole. Engineering Mechanics 18 (2), 14–20.

Gao, S.W., Wang, Y.S., Zhang, Z.M., Ma, X.R., 2005. Dual reciprocity boundary element method for flexural waves in thin plate with cutout. Applied Mathematics and Mechanics 26 (12), 1564–1573.

Hayir, A., Bakirtas, I., 2004. A note on plate having a circular cavity excited by plane harmonic SH waves. Journal of Sound and Vibration 271, 241–255.

Hu, C., Ma, X.R., Huang, W.H., 1998. Dynamic stress concentrations in thin plates with two circular cutouts. Acta Mechanica Sinica 30 (5), 587–596.

Hu, C., Fang, X.Q., Huang, W.H., 2007. Multiple scattering of flexural waves in a semi-infinite thin plate with a cutout. International Journal of Solids and Structures 44, 436–446.

Kamiya, N., Kita, E., 1995. Trefftz method: an overview. Advances in Engineering Software 24, 3–12.

Kung, George C.S., 1964. Dynamical stress concentration in an elastic plate. M.S. Thesis, Cornell University, Ithaca, NY.

Lee, W.M., Chen, J.T., 2008. Scattering of flexural wave in thin plate with multiple holes by using the null-field integral equation approach. CMES-Computer Modeling in Engineering & Sciences 37 (3), 243–273.

Liu, D., Gai, B., Tao, G., 1982. Applications of the method of complex functions to dynamic stress concentrations. Wave Motion 4, 293–304.

Linton, C.M., Evans, D.V., 1990. The interaction of waves with arrays of vertical circular cylinders. Journal of Fluid Mechanics 215, 549–569.

Martin, P.A., 2006. Multiple Scattering Interaction of Time-Harmonic Wave with N obstacles. Cambridge University Press, UK.

Nishimura, G., Jimbo, Y., 1955. A dynamical problem of stress concentration. Journal of the Faculty of Engineering, University of Tokyo, Japan 24, 101.

Norris, A.N., Vemula, C., 1995. Scattering of flexural waves on thin plates. Journal of Sound and Vibration 181, 115–125.

Pao, Y.H., Mow, C.C., 1972. Diffraction of Elastic Waves and Dynamics Stress Concentration. Crane, New York.

Pao, Y.H., 1962. Dynamical stress concentration in an elastic plate. Transactions of the ASME Journal of Applied Mechanics 29, 299–305.

Squire, V.A., Dixon, T.W., 2000. Scattering of flexural waves from a coated cylindrical anomaly in a thin plate. Journal of Sound and Vibration 236 (2), 367–373.

Trefftz, E., 1926. Ein Gegensttick zum Ritz' schen Verfahren. In: Proc. Second Int. Cong. Appl. Mech., Zurich, pp. 131–137.

Watson, G.N., 1995. A Treatise on the Theory of Bessel Functions, Second ed. Cambridge Library edition, Cambridge.

Zaviška, F., 1913. die Beugung elektromagnetischer Wellen an parallelen, unendlich langen Kreiszylindern. Annalen der Physik 4 (Folge 40), 1023–1056.